Research Article | Vol. 27, No. 20 / 30 September 2019 / Optics Express 28855
Optics EXPRESS

Third-harmonic generation in multilayer Tin Diselenide under the influence of Fabry-Perot interference effects

RABINDRA BISWAS, MEDHA DANDU, SRUTI MENON, KESHAV KUMAR JHA, JYOTHSNA K. M., KAUSIK MAJUMDAR, AND VARUN RAGHUNATHAN*

Department of Electrical Communication Engineering, Indian Institute of Science, Bangalore 560012, India
*varunr@iisc.ac.in

Abstract: Two-dimensional layered materials are in general known to exhibit strong layer dependent nonlinear optical response owing to the crystal symmetry and associated phase matching considerations. Here we report up-conversion of 1550 nm incident light using third-harmonic generation (THG) in multilayered tin di-selenide ($SnSe_2$) and study its thickness dependence by simultaneously acquiring spatially-resolved images in the forward and backward propagation direction. We find good agreement between the experimental measurements and a coupled-wave equation model we have developed when including the effect of Fabry-Perot interference between the $SnSe_2$ layer and the surrounding medium. We extract the magnitude of the third order electronic nonlinear optical susceptibility of $SnSe_2$, for the first time to our knowledge, by comparing its nonlinear response with a glass substrate and find this to be ~1500 times higher than that of glass. We also study the polarization dependence and find good agreement with the expected angular dependence of nonlinear polarization considering the crystal symmetry of $SnSe_2$. The large nonlinear optical susceptibility of multi-layer $SnSe_2$ makes it a promising material for studying nonlinear optical effects. This work demonstrates that in addition to the large inherent nonlinear optical susceptibility, the high refractive index of these materials and optical absorption above the bandgap strongly influence the overall nonlinear optical response and its thickness dependence characteristics.

1. Introduction

Layered materials such as graphene, transition metal dichalcogenide (TMDC), black phosphorus, etc. are being considered as potential candidates for realizing ultrathin nonlinear photonic devices for applications in wavelength up-conversion, wavelength mixing, saturable absorption, optical limiting etc. [1]. The unique optoelectronic properties of these materials, such as layer tunable bandgap [2], room temperature excitonic resonances [3,4], layer dependent lattice symmetry [5], strong nonlinear response [1], and high optical damage threshold with fluence on the order of 50-300 mJ/cm^2 [6] motivate the study of nonlinear optical processes in these materials. The high refractive index of TMDC multi-layered material and the associated increased effective optical path length has been utilized previously for realizing ultrathin linear optical elements, such as gratings and lenses [7] and also for enhancing Raman scattering [8]. In the context of nonlinear optics, a direct consequence of the high refractive index of the layered material in comparison to the surrounding is the strong Fabry-Perot interference effects between the forward and backward propagating waves at both the excitation and nonlinear emission wavelengths inside the layered material [9].

In order to characterize the inherent nonlinear optical response from such high refractive index layered materials, multiphoton microscopy techniques are particularly useful in spatially resolving the nonlinear signal and correlating this to the layer thickness, crystal symmetry and

#369215 https://doi.org/10.1364/OE.27.028855
Journal © 2019 Received 4 Jun 2019; revised 28 Aug 2019; accepted 3 Sep 2019; published 24 Sep 2019

Optics EXPRESS

linear optical properties. Harmonic generation microscopy using second, and third-harmonic generation processes as the contrast mechanism can be used to characterize thickness dependent nonlinear response, identify defects, grain boundaries, and also determine in-plane crystal orientation [10]. Second harmonic generation from monolayer and multilayer TMDCs [11–14], hexagonal Boron nitride (h-BN) [15], Gallium selenide [16] and third harmonic generation from Molybdenum and Tungsten based TMDCs [17–19], Graphene [20], Rhenium di-sulfide (ReS_2) [21], Tin di-sulphide (SnS_2) [22] and black phosphorus [23,24] have been studied in the past. In this paper, we study third harmonic generation (THG) and quantify the third-order parametric nonlinear optical effects from multilayer tin di-selenide ($SnSe_2$), a largely unexplored layered material for photonic applications.

$SnSe_2$ crystal is a group IVA-VIA semiconductor with CdI_2-type lattice, found predominantly in 1T phase with hexagonal stacking and $P3\bar{m}1$ space group [25,26]. It exhibits an indirect bandgap of ~ 1.1 eV which is tunable with layer thickness. This band gap results in material absorption and high refractive index (typically > 3) in the visible and near-infrared wavelength range (< 1.12 µm) [27, 28]. The linear optical properties have a direct impact on the optoelectronic applications of $SnSe_2$ layered material, for example as standalone [29–31] and heterostructure [32–34] photodetectors exhibiting strong light absorption. In the context of nonlinear optical effects, few-layer $SnSe_2$ has been used as saturable absorbers for Q-switched pulsed laser at 1 µm wavelength utilizing intensity dependent two-photon absorption process [35]. We have recently reported enhanced single- and two-photon photoluminescence from $MoS_2/SnSe_2$ heterostructures [36], where absorption in $SnSe_2$ coupled with a near resonant energy transfer process to less absorbing MoS_2 results in strong photoluminescence from MoS_2 monolayer. There has also been previous reports of nonlinear optical studies on ternary chalcogenides of Ge-Sn-Se [37]. Here, we study the thickness dependent directional THG emission from multilayer $SnSe_2$ by simultaneously imaging both forward and backward propagating THG signals. Good agreement is obtained with a nonlinear coupled-wave propagation model when including the effect of strong Fabry-Perot interference for both fundamental and THG wavelength, and material absorption at the THG wavelength. We extract the value of the electronic third-order nonlinear susceptibility coefficient by comparing the nonlinear optical response of $SnSe_2$ with a glass substrate and obtain the third order susceptibility to be ~ 1500 times larger than glass. We also investigate the polarization dependence of THG emission and compare it with the expected angular dependence of nonlinear polarization considering the known crystal symmetry of $SnSe_2$. The thickness dependent THG study presented here can potentially aid in determining optimal multi-layer thickness of $SnSe_2$, taking into account realistic linear optical effects for realizing efficient layered material based nonlinear photonic devices. This work also emphasizes the importance of the interplay between the linear (high refractive index and material absorption) and nonlinear optical effects in determining the overall nonlinear optical response from layered material systems.

2. Experimental studies

The nonlinear optical microscopy set-up used for THG imaging of $SnSe_2$ samples is shown in Fig. 1(a). The third harmonic signal at 516.6 nm emitted both in the forward and backward (epi) directions (as shown in Fig. 1(b)) are collected simultaneously to form images. An optical parametric oscillator (Levante IR) pumped by a femtosecond fiber laser at 1040nm (Fidelity HP) is used as a source of fundamental excitation at 1550 nm wavelength with 200 fsec pulse width and 80MHz repetition rate. The $SnSe_2$ sample is mounted on an Olympus IX73 inverted microscope with the fundamental excitation focused using a 20x/0.75 NA objective, illuminating ~50% of the back aperture of the objective. The optical resolution at the THG emission wavelength is estimated to be ~770 nm. A combination of half-wave plate and polarizer has been used to control the power and the polarization of the incident beam. For the backward configuration, the same objective lens is used to collect the THG and then separated from the pump using a dichroic mirror.

Optics EXPRESS

The backward THG is then detected using a photomultiplier tube (Hamamatsu R3896) with a set of bandpass (520 ± 20nm) and short-pass (890nm) filter mounted in front to reject any residual pump and to minimize any stray light. In the forward configuration, a 0.55 NA condenser is used to collect the forward THG and then detected using another photomultiplier tube (Hamamatsu R2658) with a similar set of filters as used in the backward. A pair of galvanometric mirrors (Thorlabs GVS002) was used to scan the laser beam to obtain two-dimensional third harmonic images of $SnSe_2$ flake.

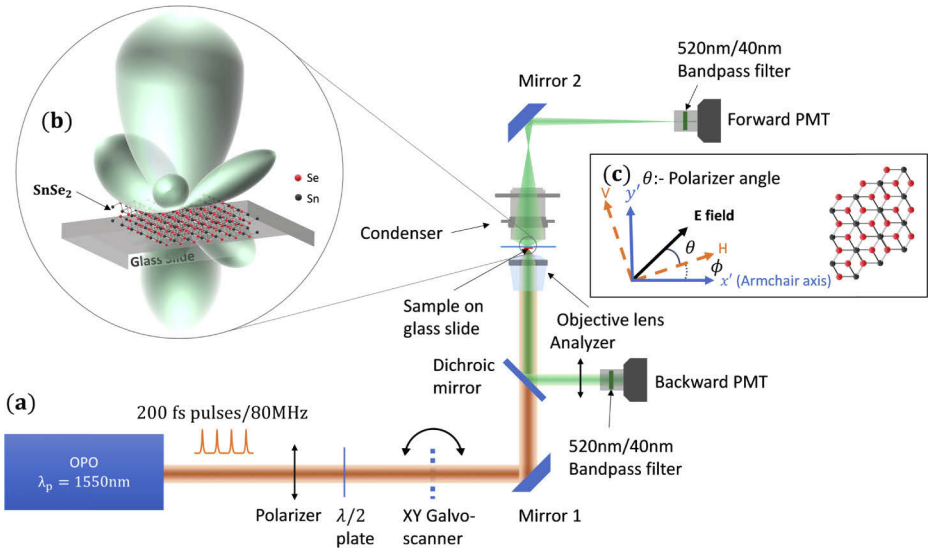

Fig. 1. (a) Schematic of the nonlinear microscopy setup used for THG imaging. (b) Schematic rendering of the third harmonic radiation pattern emitted in both forward and backward directions from $SnSe_2$ layered material on a glass slide. (c) The orientation of the crystallographic axis (in blue), lab axis (in orange dashed) at an angle ϕ relative to the crystal axis and the orientation of the incident electric field (in black) at an angle θ relative to the lab axis is shown.

Experiments were performed on a $SnSe_2$ flake exfoliated onto a glass slide. The $SnSe_2$ sample was prepared using Scotch tape transfer technique, where we exfoliated $SnSe_2$ in bulk form onto a glass slide with a Poly-dimethylsiloxane (PDMS) layer. A suitable flake with a varying number of layers is identified using an optical microscope and transferred onto a glass substrate. The varying layer thickness is verified using color contrast in the optical microscopy images and the thickness maps obtained using AFM images, as shown in Figs. 2(a) and 2(b) respectively. Figures 2(c) and 2(d) shows the forward and backward THG images respectively for an incident power level of 5.5 milli-watt, with the colorbar scale denoting the THG signal as a PMT voltage. With the excitation beam focused on the $SnSe_2$ flake, the background THG signal from the glass/silicon substrate is found to be 1000 times weaker than $SnSe_2$, thus resulting in negligible interference between the nonlinear signal generated in the $SnSe_2$ layer and the bottom substrate. The forward and backward THG images visually show intricate thickness dependence. However, the two images show very different contrast and hence thickness dependence. This effect is analyzed in detail using nonlinear coupled-wave equation model in section III below. Thickness dependence of THG emission has been observed previously in ReS_2 [21] and black phosphorus [23], however THG measurements were performed only in the backward emission direction and no comparison with the forward THG emission were studied.

Optics EXPRESS

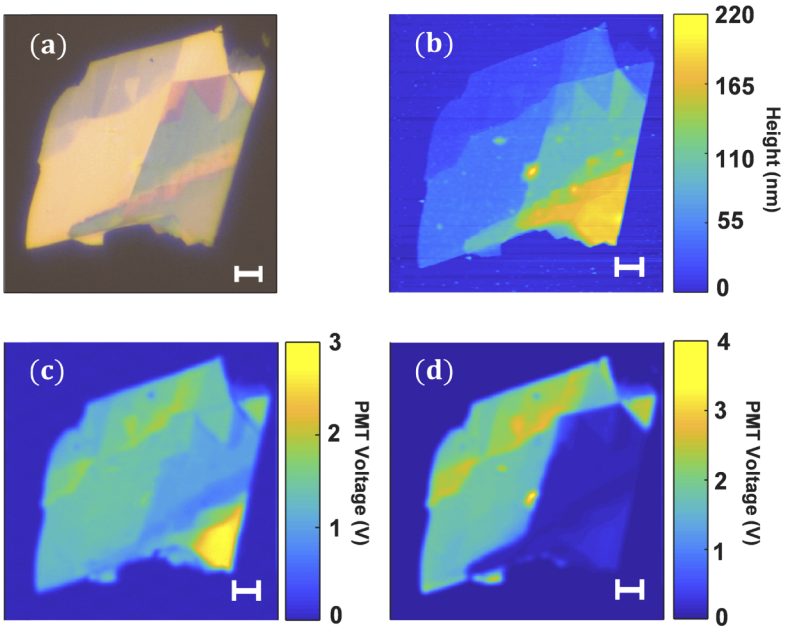

Fig. 2. (a) Optical microscopy image, (b) AFM image, (c) forward THG image and, (d) backward THG image for the $SnSe_2$ layer on a glass slide. Scale bar shown in the images is 5 μm.

The nonlinear signal collected from the $SnSe_2$ flake is verified to be third-harmonic by measuring the power dependence of the output THG signal as a function of incident fundamental power. The log-log plot of this power dependence shown in Fig. 3(a) with a slope of 3.08, confirming the THG process. Next, polarization studies were performed on ~ 30 nm region of the flake by rotating the incident polarization of the fundamental using a half-wave plate while keeping the analyzer before the PMT either aligned parallel (denoted H) or perpendicular (denoted V) to the lab co-ordinates, as shown in Fig. 1(c). The polar plot representing the THG signal as a function of the fundamental polarization angle for the two different analyzer orientations is shown in Fig. 3(b). Considering the space group of $SnSe_2$, the non-zero third-order optical susceptibility elements are: xxxx = yyyy = xxyy + xyyx + xyxy, with xxyy = yyxx, xyyx = yxxy, xyxy = yxyx [38]. The z- dependent components are neglected in the above listing as longitudinal polarized field components are negligible at the fundamental and third harmonic wavelengths. The nonlinear polarization of interest as a function of incident fundamental field, E(ω) for the two different analyzer orientations are obtained as:

$$P_H^{(3)}(3\omega) = \epsilon_o \chi_{xxxx}^{(3)} E^3(\omega).\, Cos(\theta) \tag{1}$$

$$P_V^{(3)}(3\omega) = \epsilon_o \chi_{xxxx}^{(3)} E^3(\omega).\, Sin(\theta) \tag{2}$$

The THG signal which is proportional to the absolute value squared of the nonlinear polarization follows sinusoidal dependence (orange and black solid curves) and shows good agreement with experimental data (red and green circles), as shown in Fig. 3(b). The sum of the two polarized THG data shows close to circular symmetry (light blue circles). The polarization study shows that for the thickness under consideration the $SnSe_2$ flake exhibits nonlinear properties similar to bulk $SnSe_2$.

The THG signal obtained from $SnSe_2$ region for thickness in the range of 20–50 nm is compared with a 500μm thick BK7 glass substrate for an incident average power level of 2.6 milli-watt.

Optics EXPRESS

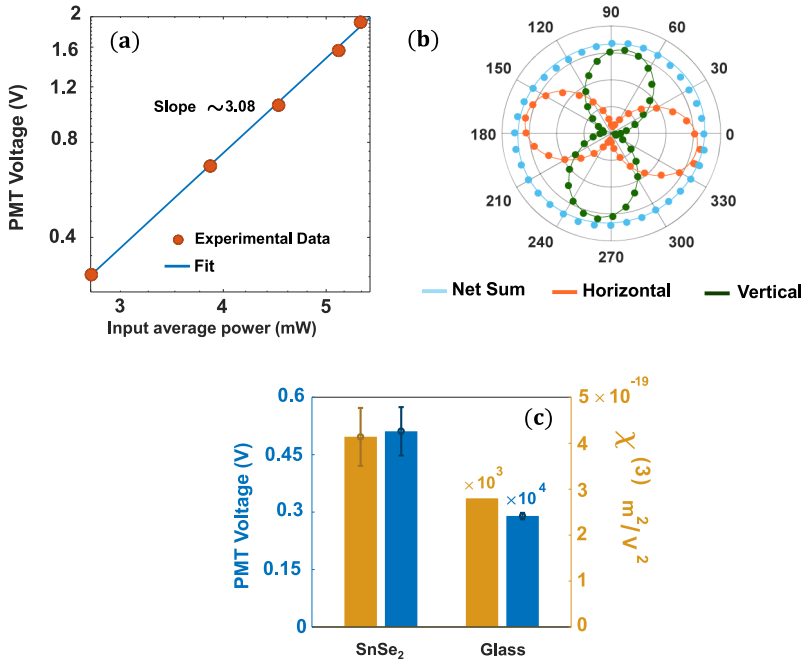

Fig. 3. (a) Power dependence of the THG signal measured as PMT voltage as a function of input incident average power level. (b) Polarization dependent THG measurements for analyzer before the PMT oriented in the horizontal (orange) and vertical (dark green) directions and sum of the two (blue). The solid curves denote the fit to the experimental data. (c) Comparison of the THG signal (left axis – blue color) and third-order nonlinear optical susceptibility, (right axis – orange color) between $SnSe_2$ flake and glass substrate.

For the case of the glass substrate, the maximum THG signal is obtained when the glass-air interface overlaps with the beam waist, as has been observed in previous THG experiments on samples with axial interfaces [39–41]. This results in the THG interaction length corresponding to approximately a Rayleigh length ($z_o = 1.1$ μm). The comparison of the THG signal strength is shown in Fig. 3(c) with $SnSe_2$ layer generating on an average 1760 times stronger THG than the glass substrate. The relative magnitudes of the THG signal are used to extract the third-order nonlinear optical susceptibility of $SnSe_2$ using the nonlinear coupled-wave propagation model, as discussed below.

3. Nonlinear coupled-wave propagation model

To extract the nonlinear optical susceptibility and to understand the observed thickness dependence of THG, we model the THG generation in the $SnSe_2$ layer using nonlinear coupled-wave analysis. At the incident fundamental wavelength, the field profile inside the $SnSe_2$ layer in the presence of reflection from the $SnSe_2$ and glass/ air interface is given as:

$$E_{1s}(\omega, z) = \frac{t_{as}(e^{-ik_1 z} + r_{sg}e^{-ik_1(2d_1 - z)})}{1 + r_{as}r_{sg}e^{-2ik_1 d_1}} E_{1a}^{+} \tag{3}$$

where, E_{1a}^{+} denotes the forward propagating incident fundamental field in air, as shown in the schematic of Fig. 4, with the terms $e^{-ik_1 z}$ and $e^{ik_1 z}$ in the numerator representing the forward and backward propagating fundamental fields respectively, with fundamental wavevector, k_1. The incident peak optical intensity can be written as: $I_{1a}^{+} = 2c\epsilon_0 n_1 |E_{1a}^{+}|^2$. The terms r_{ij} and

Optics EXPRESS

t_{ij} correspond to the field reflection and transmission coefficient at the air-$SnSe_2$ (ij = as) and $SnSe_2$-glass (ij = sg) interface. The refractive index (n) and extinction coefficient (κ) used in this analysis are taken from [27] with values of (n,κ) given as: (3.22,0) and (3.43,1.46) for the fundamental and THG wavelengths respectively. The reflection from glass substrate/ air interface is ignored here as the refractive index difference is small to cause significant feedback. The third order nonlinear polarization at the third-harmonic wavelength which acts as the driving force to generate the THG field in the sample is given as:

$$P^{(3)}(3\omega, z) = \epsilon_0 \chi^{(3)} {E_{1s}}^3(\omega, z) =$$

$$\epsilon_0 \chi^{(3)} \frac{t_{as}^3}{\left(1 + r_{as} r_{sg} e^{-ik_1 d_1}\right)^3} E_{1a}^{+3} \left(e^{-ik_1 3z} + r_{sg}^3 e^{-ik_1 6d_1} e^{ik_1 3z} \; + \; 3 r_{sg} e^{-ik_1 2d_1} e^{-ik_1 z} + \; 3 r_{sg}^2 e^{-ik_1 4d_1} e^{ik_1 z}\right) \tag{4}$$

The third order nonlinear polarization shown above is expanded into four terms which include the THG emission arising from: (i) three forward propagating fundamental photons, (ii) three backward propagating fundamental photons, (iii) two forward and one backward propagating fundamental photons, and (iv) one forward and two backward propagating fundamental photons respectively. A direct consequence of the Fabry-Perot interference effects is the creation of new wave-mixing terms (last two terms) that result in THG emission [40]. This is to be contrasted with conventional THG without the interference effect which considers only the first two terms [38].

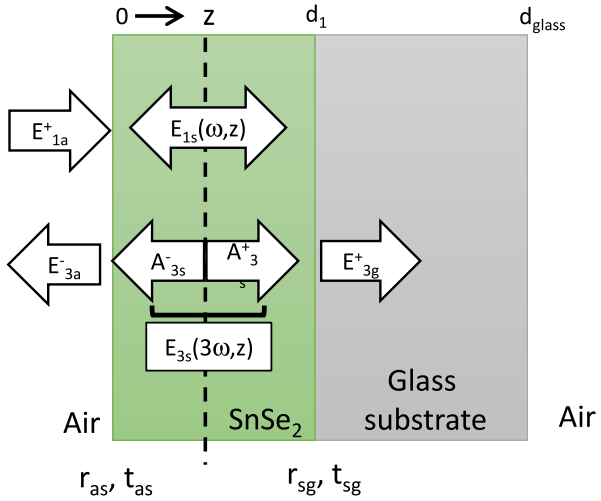

Fig. 4. Schematic of the $SnSe_2$ flake on glass substrate showing the incident electric fields (denoted with subscript 1) and generated THG fields (denoted with subscript 3) in each region. Thickness of the $SnSe_2$ flake and glass substrate are denoted as d_1 and d_{glass} respectively.

The third harmonic field generated can be expanded as: $E_{3s}(3\omega, z) = A_{3s}^{+} e^{-ik_3 z} + A_{3s}^{-} e^{ik_3 z}$, denoting the forward and backward propagating THG respectively inside the $SnSe_2$ layer with wavevector, k_3. The time-dependent phase term, $e^{i3\omega t}$ is not explicitly written above. The coupled-wave equations representing the nonlinear wave propagation used to model the backward and forward propagating THG along the layered material can be written as [38]:

$$2ik_3 \frac{dA_3^{-}}{dz} e^{ik_3 z} = -\frac{\omega_3^2}{\epsilon_0 c^2} P^{(3)}(3\omega, z) \tag{5}$$

Optics EXPRESS

$$-2ik_3\frac{dA_3^+}{dz}e^{-ik_3z} = -\frac{\omega_3^2}{\epsilon_0 c^2}P^{(3)}(3\omega, z) \tag{6}$$

The coupled-wave equations are solved numerically to obtain the THG field amplitude of the form: $\widetilde{A_3^+} = A_3^+ e^{-ik_3z}$ and $\widetilde{A_3^-} = A_3^- e^{ik_3z}$, representing the forward and backward propagating THG including the effect of phase accumulation and attenuation at the THG wavelength along the propagation direction. The forward and backward propagating field amplitudes at the exit of the $SnSe_2$ and glass/ air interface under the influence of Fabry-Perot interference for the third harmonic wavelength are given as:

$$E_{3g}^+(d_1) = t'_{sg}\frac{\widetilde{A_3^+}(d_1) + r'_{sa}\widetilde{A_3^-}(0)\,e^{-ik_3d_1}}{1 + r'_{as}r'_{sg}e^{-2ik_3d_1}} \tag{7}$$

$$E_{3a}^-(0) = t'_{sa}\frac{\widetilde{A_3^-}(0) + r'_{sg}\widetilde{A_3^+}(d_1)e^{-ik_3d_1}}{1 + r'_{as}r'_{sg}e^{-2ik_3d_1}} \tag{8}$$

r'_{ij} and t'_{ij} represent the field reflection and transmission coefficients at the THG wavelength, with subscripts g and s on the left-hand side denoting the field amplitude in the glass and air region respectively after transmitting through the $SnSe_2$ layer. The first term in the numerators above represent the solutions to the nonlinear wave propagation differential equations representing the forward and backward THG emission respectively. The second term refers to the reflected backward and forward THG signal at the $SnSe_2$/air and $SnSe_2$/glass interfaces respectively. The peak intensity at the THG wavelength as a function of the field amplitudes is obtained as:

$$I_3^+ = 2c\epsilon_0 n_3|E_{3g}^+(d_1)|^2,\ I_3^- = 2c\epsilon_0 n_3|E_{3a}^-(0)|^2 \tag{9}$$

The average optical power is related to the peak optical intensity for pulsed excitation, assuming gaussian incident field profile as follows [21]:

$$\bar{P}_k^{+/-} = R\left(\frac{\pi}{ln2}\right)^{3/2}\frac{\tau}{2m}\left(\frac{w}{2}\right)^2 I_k^{+/-} \tag{10}$$

where the subscript k refers to 1 or 3, the fundamental or third-harmonic respectively. The factor m = 1 or $3\sqrt{3}$ for the fundamental and third-harmonic respectively, representing the reduction in the spatial and temporal profile of the third-harmonic due to cubic dependence on the fundamental field. R = 80MHz, τ = 200 fsec and w = 1.2 μm denotes the incident pulse repetition rate, pulse width and full-width half maximum of the gaussian beam profile respectively.

The third-order nonlinear optical susceptibility of $SnSe_2$ is back-calculated from the coupled-wave equation model and the comparative measurements of THG signals from $SnSe_2$ and glass substrate over their respective interaction lengths (refer to section II). For the glass substrate, Fabry-Perot interference effects are not considered due to the small refractive index difference between glass and the surrounding medium and the fact that the divergence of the incident beam is significant across the thickness of the substrate. With the knowledge of the value of $\chi^{(3)}$ for glass substrate of 2.8×10^{-22} m^2/V^2 [38] and the incident optical power level, the value of $\chi^{(3)}$for $SnSe_2$ is estimated as 4.14 +/- 0.63 x10^{-19} m^2/V^2. The thickness dependence of the nonlinear susceptibility is within the standard deviation shown above. We also extracted the nonlinear optical susceptibility for the hypothetical case of no Fabry-Perot interference effects in the simulations and obtain the susceptibility as 1.12 +/- 0.86×10^{-18} m^2/V^2. This shows that ignoring Fabry-Perot interference effects in the $SnSe_2$ layer leads to an over-estimation of the nonlinear optical susceptibility as the large THG signal is attributed to a larger nonlinear susceptibility rather than field enhancement in the sample due to interference effects. Figure 3(b) shows a comparison of the extracted nonlinear optical susceptibility for $SnSe_2$ and glass.

Optics EXPRESS

$SnSe_2$ layered material is found to exhibit a third order nonlinear optical susceptibility of ~1500 times larger than glass. A comparison of the above extracted nonlinear optical susceptibility with the values for other layered materials is summarized in Table 1. The comparison shows that the nonlinear optical response of $SnSe_2$ is of the same order of magnitude as other popular 2D materials, such as TMDCs and h-BN.

Table 1. Comparison of nonlinear optical susceptibility of various layered material

Layered Materials	$\chi^{(3)}(m^2/V^2)$	No. of Layers	Excitation Wavelength(nm)	References
Graphene	1.5×10^{-19}	Monolayer	1560	18
MoS_2	2.9×10^{-19}	Monolayer	1560	18
WSe_2	1.16×10^{-19}	Few layer	1546	19
ReS_2	5.3×10^{-18}	Multilayer	1515	21
Black Phosphorus	1.4×10^{-19}	Multilayer	1557	23
SnS_2	3.1×10^{-19}	Multilayer	1550	22
$SnSe_2$	4.14×10^{-19}	Multilayer	1550	This work

Figure 5 shows the solution to the nonlinear coupled-wave equations model both in the form of simulated THG images and plots comparing the simulations with experimental data. The simulated forward and backward images shown in Figs. 5(a) and 5(c) respectively are obtained by converting the AFM thickness map to THG signal using the above-described model. The

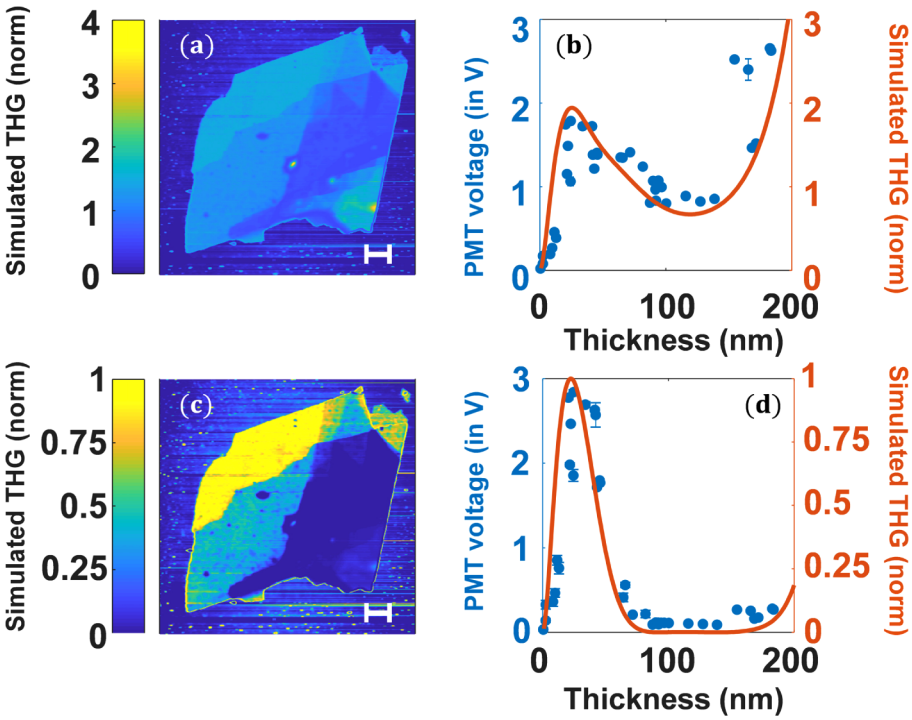

Fig. 5. Simulated images of: (a) forward THG, (c) backward THG and comparison of the experimental and simulated THG data for: (b) forward THG, and (d) backward THG. Blue solid circles denote the experimental data and the orange solid curve denotes the simulation results. Scale bar shown in the images is 5 µm.

Optics EXPRESS

experimental data (blue circles) is compared with the simulated plots (red solid curves) in Figs. 5(b) and 5(d) for the forward and backward THG respectively with the simulation results normalized by the backward THG peak. There is good agreement between the experimental PMT voltage and the normalized simulation results. Both forward and backward THG signals are found to exhibit a peak at a nominal layer thickness of 25–30 nm followed by a decrease, and a subsequent increase for thickness > 100 nm. The characteristic shape of the thickness dependent THG for both forward and backward emission arises due to Fabry-Perot interference effect and material absorption at the THG wavelength. This effect is found to be more significant when compared to the typical oscillatory behavior expected for the nonlinear signal with length due to phase mismatch, with coherence length calculated as ~ 38 nm and 1.23 μm for backward and forward THG respectively [38]. The simulation results of the forward and backward THG emission clearly shows the importance of linear optical effects in particular, Fabry-Perot interference in explaining the observed thickness dependence. Moreover, the backward THG is found to be more sensitive to thickness variation than the forward THG resulting in enhanced image contrast for lower thicknesses, as has been observed in the experimental THG images of Figs. 2(c) and 2(d) and supported by the simulations. This is attributed to the large variation in backward THG for small changes in thickness due to larger phase mismatch, as shown in Figs. 5(d). The relative increase in THG signal with increasing layer thickness is however more pronounced for forward THG when compared to backward THG due to lower phase mismatch for forward generated THG. In this analysis, we have not performed quantitative comparisons between the forward and backward THG signals as the two PMTs used are of different specifications and the path loss for the forward and backward collection are also very different.

In the theoretical model, we ignore any depletion or saturable absorption effects experienced by the fundamental excitation beam. This is justified for the film thickness under consideration in this work (10–200 nm) and weak conversion efficiency (on the order of 10^{-6}%). For higher thicknesses or conversion efficiencies, the pump depletion effect would have been be included in the coupled-wave equation model, as has been experimentally observed in nonlinear optical studies in millimeter thick Zinc Selenide samples [42]. It should be emphasized the nonlinear wave propagation model considered above assumes slowly varying amplitude approximation (SVAA) which is valid for amplitude variations much smaller than the wavelength in the medium [38,43], which is questionable for 2D layered materials of thickness as considered in this work in the presence of strong interference effects. The simulations with SVAA show good overall agreement with the experimental data in Figs. 2(c) and 2(d), thus justifying the use of SVAA here. Modeling the nonlinear wave propagation in 2D layered materials beyond SVAA will be considered in a future report. The nonlinear wave propagation model described above also ignores the role of Guoy phase shift of focused gaussian excitation beam. Guoy phase shift has been considered previously in the context of THG microscopy to explain selective longitudinal interfacial contrast [44]. However, when considering tens of nanometer layered material, the inverse tangential variation of the Guoy phase shift [45] can be approximated as a linear dependence: $Tan^{-1}\left(\frac{z}{z_o}\right) \approx \frac{z}{z_o} \ll kz$, where z_o is the Rayleigh length. Thus, the effect of the Guoy phase shift on the phase mismatch can be ignored for the range of layer thickness under considered here.

4. Conclusions

In conclusion, 2D layered $SnSe_2$ is a promising candidate for realizing ultrathin nonlinear photonic device for wave-mixing application. This is supported by the large measured nonlinear optical susceptibility, $\chi^{(3)} = 4.14 \times 10^{-19}$ m^2/V^2, which is found to be ~ 1500 times larger than glass. The THG emission from $SnSe_2$ is found to exhibits intricate thickness dependence in both forward and backward THG microscopy images, with very different image contrast. This is explained using a

Optics EXPRESS

nonlinear wave propagation model in the presence of material absorption at the THG wavelength and Fabry-Perot interference effects at the fundamental and THG wavelengths due to the refractive index difference between the layered material and the surrounding medium. This study clearly points to the interplay between linear and nonlinear optical effects occurring in layered materials strongly influencing the overall nonlinear optical response and its layer dependence. Even though monolayer 2D materials are interesting for the study of basic nonlinear optical physics, multi-layer materials are promising for practical nonlinear optical device applications, especially in the context of third-order nonlinear optical processes. The present study can potentially be used in this context in determining optimal multi-layer 2D material thickness for realizing efficient nonlinear photonic devices in the presence of realistic linear optical effects. Such nonlinear photonic devices can potentially be designed as standalone layers on a substrate as presented here or as heterostructure in the presence of other 2D materials [36] and resonant nanophotonic structures [46] or waveguides to achieve longer interaction lengths [47].

Funding

Science and Engineering Research Board (ECR/2016/001591).

Acknowledgments

We thank Asish Prosad for helping with the third harmonic generation microscopy experiments.

References

1. A. Autere, H. Jussila, Y. Dai, Y. Wang, H. Lipsanen, and Z. Sun, "Nonlinear Optics with 2D layered Materials," Adv. Mater. **30**(24), 1705963 (2018).
2. W. S. Yun, S. Han, S. C. Hong, I. G. Kim, and J. Lee, "Thickness and strain effects on electronic structures of transition metal dichalcogenides: 2H-MX_2 semiconductors (M = Mo, W; X = S, Se, Te)," Phys. Rev. B **85**(3), 033305 (2012).
3. L. C. Flatten, Z. He, D. M. Coles, A. A. Trichet, A. Powell, R. A. Taylor, J. H. Warner, and J. M. Smith, "Room-temperature exciton-polaritons with two-dimensional WS_2," Sci. Rep. **6**(1), 33134 (2016).
4. S. Das, G. Gupta, and K. Majumdar, "Layer degree of freedom for excitons in transition metal dichalcogenides," Phys. Rev. B **99**(16), 165411 (2019).
5. Y. Li, Y. Rao, K. F. Mak, Y. You, S. Wang, C. R. Dean, and T. F. Heinz, "Probing symmetry properties of few-layer MoS_2 and h-BN by optical second-harmonic generation," Nano Lett. **13**(7), 3329–3333 (2013).
6. I. Paradisanos, E. Kymakis, C. Fotakis, G. Kioseoglou, and E. Stratakis, "Intense femtosecond photoexcitation of bulk and monolayer MoS_2," Appl. Phys. Lett. **105**(4), 041108 (2014).
7. J. Yang, Z. Wang, F. Wang, R. Xu, J. Tao, S. Zhang, Q. Qin, B. Luther-Davies, C. Jagadish, Z. Yu, and Y. Lu, "Atomically thin optical lenses and gratings," Light: Sci. Appl. **5**(3), e16046 (2016).
8. H. Zhang, Y. Wan, Y. Ma, W. Wang, Y. Wang, and L. Dai, "Interference effect on optical signals of monolayer MoS_2," Appl. Phys. Lett. **107**(10), 101904 (2015).
9. A. Kudryavtsev, S. Lavrov, A. Shestakova, L. Kulyuk, and E. Mishina, "Second harmonic generation in nanoscale films of transition metal dichalcogenide: Accounting for multipath interference," AIP Adv. **6**(9), 095306 (2016).
10. L. Karvonen, A. Saynatjoki, M. J. Huttunen, A. Autere, B. Amirsolaimani, S. Li, R. A. Norwood, N. Peyghambarian, H. Lipsanen, G. Eda, K. Kieu, and Z. Sun, "Rapid visualization of grain boundaries in monolayer MoS_2 by multiphoton microscopy," Nat. Commun. **8**(1), 15714 (2017).
11. N. Kumar, S. Najmaei, Q. Cui, F. Ceballos, P. M. Ajayan, J. Lou, and H. Zhao, "Second harmonic microscopy of monolayer MoS_2," Phys. Rev. B **87**(16), 161403 (2013).
12. J. Ribeiro-Soares, C. Janisch, Z. Liu, A. Elias, M. Dresselhaus, M. Terrones, L. Cancado, and A. Jorio, "Second harmonic generation in WSe_2," 2D Mater. **2**(4), 045015 (2015).
13. W. T. Hsu, Z. A. Zhao, L. J. Li, C. H. Chen, M. H. Chiu, P. S. Chang, Y. C. Chou, and W. H. Chang, "Second harmonic generation from artificially stacked transition metal dichalcogenide twisted bilayers," ACS Nano **8**(3), 2951–2958 (2014).
14. C. Janisch, Y. Wang, D. Ma, N. Mehta, A. L. Elias, N. Perea-Lopez, M. Terrones, V. Crespi, and Z. Liu, "Extraordinary second harmonic generation in tungsten disulfide monolayers," Sci. Rep. **4**(1), 5530 (2015).
15. M. C. Lucking, K. Beach, and H. Terrones, "Large second harmonic generation in alloyed TMDs and boron nitride nanostructures," Sci. Rep. **8**(1), 10118 (2018).
16. X. Zhou, J. Cheng, Y. Zhou, T. Cao, H. Hong, Z. Liao, S. Wu, H. Peng, K. Liu, and D. Yu, "Strong second-harmonic generation in atomic layered GaSe," J. Am. Chem. Soc. **137**(25), 7994–7997 (2015).

Optics EXPRESS

17. R. Wang, H. C. Chien, J. Kumar, N. Kumar, H. Y. Chiu, and H. Zhao, "Third-harmonic generation in ultrathin films of MoS_2," ACS Appl. Mater. Interfaces **6**(1), 314–318 (2014).
18. R. Woodward, R. Murray, C. Phelan, R. De Oliveira, T. Runcorn, E. Kelleher, S. Li, E. De Oliveira, G. Fechine, G. Eda, and C. De Matos, "Characterization of the second-and third-order nonlinear optical susceptibilities of monolayer MoS_2 using multiphoton microscopy," 2D Mater. **4**(1), 011006 (2016).
19. H. G. Rosa, Y. W. Ho, I. Verzhbitskiy, M. J. Rodrigues, T. Taniguchi, K. Watanabe, G. Eda, V. M. Pereira, and J. C. Gomes, "Characterization of the second-and third-harmonic optical susceptibilities of atomically thin tungsten diselenide," Sci. Rep. **8**(1), 10035 (2018).
20. G. Soavi, G. Wang, H. Rostami, D. G. Purdie, D. De Fazio, T. Ma, B. Luo, J. Wang, A. K. Ott, D. Yoon, and S. A. Bourelle, "Broadband, electrically tunable third-harmonic generation in graphene," Nat. Nanotechnol. **13**(7), 583–588 (2018).
21. Q. Cui, R. A. Muniz, J. Sipe, and H. Zhao, "Strong and anisotropic third-harmonic generation in monolayer and multilayer ReS_2," Phys. Rev. B **95**(16), 165406 (2017).
22. A. Petris, P. S. Gheorghe, V. I. Vlad, E. Rusu, V. V. Ursaki, and I. M. Tiginyanu, "Ultrafast third-order optical nonlinearity in SnS_2 layered compound for photonic applications," Opt. Mater. **76**, 69–74 (2018).
23. N. Youngblood, R. Peng, A. Nemilentsau, T. Low, and M. Li, "Layer-tunable third-harmonic generation in multilayer black phosphorus," ACS Photonics **4**(1), 8–14 (2017).
24. M. J. L. F. Rodrigues, C. J. S. De Matos, Y. W. Ho, H. Peixoto, R. E. P. De Oliveira, H. Y. Wu, A. H. C. Neto, and J. Viana-Gomes, "Resonantly increased optical frequency conversion in atomically thin black phosphorus," Adv. Mater. **28**(48), 10693–10700 (2016).
25. B. Evans and R. Hazelwood, "Optical and electrical properties of $SnSe_2$," J. Phys. D: Appl. Phys. **2**(11), 1507–1516 (1969).
26. J. M. Gonzalez and I. I. Oleynik, "Layer-dependent properties of SnS_2 and $SnSe_2$ two-dimensional materials," Phys. Rev. B **94**(12), 125443 (2016).
27. M. El-Nahass, "Optical properties of tin diselenide films," J. Mater. Sci. **27**(24), 6597–6604 (1992).
28. E. P. Mukhokosi, S. B. Krupanidhi, and K. K. Nanda, "Band Gap Engineering of Hexagonal $SnSe_2$ Nanostructured Thin Films for Infra-Red Photodetection," Sci. Rep. **7**(1), 15215 (2017).
29. Y. Huang, K. Xu, Z. Wang, T. A. Shifa, Q. Wang, F. Wang, C. Jiang, and J. He, "Designing the shape evolution of $SnSe_2$ nanosheets and their optoelectronic properties," Nanoscale **7**(41), 17375–17380 (2015).
30. P. Yu, X. Yu, W. Lu, H. Lin, L. Sun, K. Du, F. Liu, W. Fu, Q. Zeng, Z. Shen, C. Jin, Q. J. Wang, and Z. Liu, "Fast photoresponse from 1 T tin diselenide atomic layers," Adv. Funct. Mater. **26**(1), 137–145 (2016).
31. X. Zhou, L. Gan, W. Tian, Q. Zhang, S. Jin, H. Li, Y. Bando, D. Golberg, and T. Zhai, "Ultrathin $SnSe_2$ Flakes Grown by Chemical Vapor Deposition for High Performance Photodetectors," Adv. Mater. **27**(48), 8035–8041 (2015).
32. K. Murali, M. Dandu, S. Das, and K. Majumdar, "Gate-tunable $WSe_2/SnSe_2$ backward diode with ultrahigh-reverse rectification ratio," ACS Appl. Mater. Interfaces **10**(6), 5657–5664 (2018).
33. K. Murali and K. Majumdar, "Self-Powered, Highly Sensitive, High-Speed Photodetection Using ITO/WSe_2 /$SnSe_2$ Vertical Heterojunction," IEEE Trans. Electron Devices **65**(10), 4141–4148 (2018).
34. X. Zhou, N. Zhou, C. Li, H. Song, Q. Zhang, X. Hu, L. Gan, H. Li, J. Lü, J. Luo, J. Xiong, and T. Zhai, "Vertical heterostructures based on $SnSe_2/MoS_2$ for high performance photodetectors," 2D Mater. **4**(2), 025048 (2017).
35. C. Cheng, Z. Li, N. Dong, J. Wang, and F. Chen, "Tin-diselenide as a new saturable absorber for generation of laser pulses at 1μm," Opt. Express **25**(6), 6132–6140 (2017).
36. M. Dandu, R. Biswas, S. Das, S. Kallatt, S. Chatterjee, M. Mahajan, V. Raghunathan, and K. Majumdar, "Strong Single- and Two-Photon Luminescence Enhancement by Non-Radiative Energy Transfer across Layered Heterostructure," ACS Nano **13**(4), 4795–4803 (2019).
37. Y. Huang, F. Chen, B. Qiao, S. Dai, Q. Nie, and X. Zhang, "Improved nonlinear optical properties of chalcogenide glasses in Ge-Sn-Se ternary system by thermal treatment," Opt. Mater. Express **6**(5), 1644–1652 (2016).
38. R.W. Boyd, *Nonlinear optics*; (Elsevier, 2003).
39. T. Y. Tsang, "Optical third-harmonic generation at interfaces," Phys. Rev. A **52**(5), 4116–4125 (1995).
40. C. Rodriguez and W. Rudolph, "Characterization and $\chi^{(3)}$measurements of thin films by third-harmonic microscopy," Opt. Lett. **39**(20), 6042–6045 (2014).
41. C. F. Chang, H. C. Chen, M. J. Chen, W. R. Liu, W. F. Hsieh, C. H. Hsu, C. Y. Chen, F. H. Chang, C. H. Yu, and C. K. Sun, "Direct backward third-harmonic generation in nanostructures," Opt. Express **18**(7), 7397–7406 (2010).
42. R. Šuminas, A. Marcinkevičiūtė, G. Tamošauskas, and A. Dubietis, "Even and odd harmonics-enhanced supercontinuum generation in zinc-blende semiconductors," J. Opt. Soc. Am. B **36**(2), A22–A27 (2019).
43. M. H. Farzad and M. Tavassoly, "Degenerate four-wave mixing without slowly varying amplitude approximation," J. Opt. Soc. Am. B **14**(7), 1707–1715 (1997).
44. J.-X. Cheng and X. S. Xie, "Green's function formulation for third-harmonic generation microscopy," J. Opt. Soc. Am. B **19**(7), 1604–1610 (2002).
45. A.E. Siegman, *Lasers*, University Science Books, Mill valley, California, 1986.
46. T. Bucher, A. Vaskin, R. Mupparapu, F. J. Lochner, A. George, K.E. Chong, S. Fasold, C. Neumann, D-Y. Choi, F. Eilenberger, F. Setzpfandt, Y.S. Kivshar, T. Pertsch, A. Turchanin, and I. Staude, "Tailoring photoluminescence from MoS_2 monolayers by Mie-resonant metasurfaces," ACS Photonics **6**(4), 1002–1009 (2019).
47. Z. Sun, A. Martinez, and F. Wang, "Optical modulators with 2D layered materials," Nat. Photonics **10**(4), 227–238 (2016).